Title
Spatial filtering and neocortical dynamics: estimates of EEG coherence

Journal
IEEE Transactions on Biomedical Engineering, 45(7)

ISSN
0018-9294

Authors
Srinivasan, R
Nunez, PL
Silberstein, RB

Publication Date
1998-07-01

DOI
10.1109/10.686789

Spatial Filtering and Neocortical Dynamics: Estimates of EEG Coherence

Ramesh Srinivasan,* Paul L. Nunez, and Richard B. Silberstein

***Abstract*—The spatial statistics of scalp electroencephalogram (EEG) are usually presented as coherence in individual frequency bands. These coherences result both from correlations among neocortical sources and volume conduction through the tissues of the head. The scalp EEG is spatially low-pass filtered by the poorly conducting skull, introducing artificial correlation between the electrodes. A four concentric spheres (brain, CSF, skull, and scalp) model of the head and stochastic field theory are used here to derive an analytic estimate of the coherence at scalp electrodes due to volume conduction of uncorrelated source activity, predicting that electrodes within 10–12 cm can appear correlated. The surface Laplacian estimate of cortical surface potentials spatially bandpass filters the scalp potentials reducing this artificial coherence due to volume conduction. Examination of EEG data confirms that the coherence estimates from raw scalp potentials and Laplacians are sensitive to different spatial bandwidths and should be used in parallel in studies of neocortical dynamic function.**

***Index Terms*—Coherence, Laplacian, neocortical dynamics.**

I. Introduction

THE electroencephalogram (EEG) time series recorded at each electrode is a sample of a random process governed by some unknown probability laws which determine the observed dynamics. If the process is Gaussian, it is specified by its first and second moments which are the mean and the variance of the signals. The Fourier transform of the autocorrelation function of each data channel is the power spectral density function, which is an estimate of signal variance as a function of frequency [1]. Numerous studies have attributed the observed power spectrum to a generator lying beneath each electrode. This is a misleading view, since experimental EEG is spatially lowpass filtered by the poorly conducting skull. A mathematical model of this spatial filtering is developed here, showing that scalp EEG is preferentially sensitive to large correlated dipole layers. The surface Laplacian estimate of cortical surface potentials is shown to be sensitive to higher spatial frequencies, with a bandpass spatial transfer function.

The spatial statistics of scalp EEG can be characterized by a spatial autocorrelation function which is usually represented as coherence in individual frequency bands. In general, these coherences result from neocortical source correlation, volume conduction properties of the head, and reference electrode effects. A stochastic model of the spatial correlation due to volume conduction is developed here to examine the influence of the spatial filtering and reference electrode or Laplacian algorithm on coherence. Estimates of coherence from referenced potentials and Laplacian data are shown to provide complementary views of neocortical dynamics at distinct spatial scales.

Manuscript received March 22, 1996; revised February 24, 1998 The work of R. Srinivasan was supported by a National Institutes of Mental Health (NIMH) Fellowship. This work was supported by the NIMH and the National Institutes for Neurological Disease and Stroke (NINDS) under Small Business Innovation and Research (SBIR) grants to Electrical Geodesics, Inc. *Asterisk indicates corresponding author.*

*R. Srinivasan was with the Institute of Cognitive and Decision Sciences, Department of Psychology, University of Oregon, Eugene, OR 97403-1227 USA. He is now with Electrical Geodesics, Inc., Eugene, OR 97403 USA, and the Neurosciences Institute, 10640 John Jay Hopkins Drive, San Diego, CA 92121 USA (e-mail: srinivasan@nsi.edu).

P. L. Nunez is with the Brain Physics Group, Department of Biomedical Engineering, Tulane University, New Orleans, LA 70118 USA.

R. B. Silberstein is with the Brain Sciences Institute, Swinburne University of Technology, Melbourne, Vic., 3122 Australia.

Publisher Item Identifier S 0018-9294(98)04378-X.

II. Spatial Filtering of Scalp Potentials and the Surface Laplacian

Four concentric spherical shells, which represent brain, cerebrospinal fluid (CSF), skull, and scalp provide a simple physical model of the volume conduction properties of the head [2], [3]. This model has been introduced as an improvement of the three concentric spheres model of the head [2], [4]–[6], by including the CSF layer. The fundamental assumptions of the model are that Ohm's law applies in each region and that capacitive effects are negligible. In this case, the scalp potential distribution depends on the magnitudes and locations of the current sources and the thickness and conductivity of the spherical shells [7]. There is substantial variability in the thickness of the skull and scalp and head size in the adult population. In addition, skull thickness varies across different regions of the head [8]. Nevertheless, the four concentric spheres model is a valuable simulation tool which provides reasonable estimates (often within 10%–20%) of scalp potentials for brain current sources in comparisons with more realistic finite element models [9].

The EEG is generated by dipole current sources which may be distributed over the entire brain [7]. The scalp surface potential due to a radial dipole at an arbitrary location in spherical coordinates (r_z, θ', ϕ') is readily obtained from the four spheres solution and the addition theorem for spherical harmonics $Y_{nm}(\theta, \phi)$ as the Green's function [4]

$$G_{\mathrm{SCALP}}(\theta, \phi, \theta', \phi') = \sum_{n=1}^{\infty} \frac{4\pi H_n}{2n+1} \sum_{m=-n}^{n} Y_{nm}^{*}(\theta', \phi') Y_{nm}(\theta, \phi). \quad (1)$$

Here, the H_n are determined by the four concentric spheres model parameters (layer thicknesses and conductivities) and

the source distribution's radial position (r_z) as shown in the Appendix. The spherical harmonics $Y_{nm}(\theta, \phi)$ are the orthogonal basis set on a spherical surface, analogous to sinusoidal functions in the time domain, with examples shown in Fig. 1(a). The form of (1) is somewhat different for tangential dipoles, but the relative weighting of spherical harmonics is still determined by the parameters H_n, which depend only on the head model and the radial position of the source (r_z). The head model parameters are assumed to be to $(r_{\text{brain}}, r_{\text{CSF}}, r_{\text{skull}}, r_{\text{scalp}}) = (8, 8.2, 8.7, 9.2)$ cm and conductivity ratios $\sigma_{\text{brain/CSF}} = 0.2$, $\sigma_{\text{brain/skull}} = 80$, and $\sigma_{\text{brain/scalp}} = 1$. If the current distribution (source strength per unit area) at a fixed depth is $B(r_z, \theta, \phi)$, for instance macrocolumnar sources in the gyri, 2 mm below the cortical surface (i.e., $r_z = 7.8$ cm), the surface potential is obtained by multiplying the source distribution by the Green's function and integrating over the source distribution.

Any fixed depth (r_z) source distribution $B(\theta, \phi)$, can be expressed as a sum over spherical harmonics

$$B(\theta, \phi) = \sum_{n=1}^{\infty} \sum_{m=-n}^{n} B_{nm} Y_{nm}(\theta, \phi). \tag{2}$$

Multiplying the expansion equation (2) by (1) and integrating over the spherical source distribution results in

$$V_{\text{SCALP}}(\theta, \phi) = \sum_{n=1}^{\infty} \sum_{m=-n}^{n} \frac{4\pi}{2n+1} H_n B_{nm} Y_{nm}(\theta, \phi) \tag{3}$$

so that a spatial frequency domain transfer function for scalp potential can be defined as

$$T_{\text{SCALP}}(n) = \frac{4\pi}{2n+1} H_n. \tag{4}$$

The magnitude of this transfer function is plotted in Fig. 1(b) for different values of skull resistivity and CSF thickness. In all cases, volume conduction causes the well-known low-pass spatial filtering of scalp potentials. This characteristic is only slightly modified by the inclusion of a normal CSF layer and realistic variations in skull conductivity. The inclusion of tangential dipoles does not change this qualitative result as the transfer function only depends on the head model parameters and source depth, and is independent of the orientation of the source. Deeper dipole layers would be even more severely low-pass spatial filtered than is indicated by the figure. Thus, scalp potentials due to a variety of complex source distributions should be relatively homogeneous over the scalp, which is often observed experimentally [11]–[14].

High-resolution EEG techniques provide reference-independent estimates of cortical surface potential (or radial skull current density) using cortical imaging or surface Laplacian methods [4], [12], [15]–[17]. Although they have different theoretical basis, these methods provide consistent estimates of cortical surface potentials in simulations and experimental studies [15], [16]. The surface Laplacian is the second spatial derivative of potentials on the scalp surface, usually approximated by a sphere or a general ellipsoid [17]. The surface

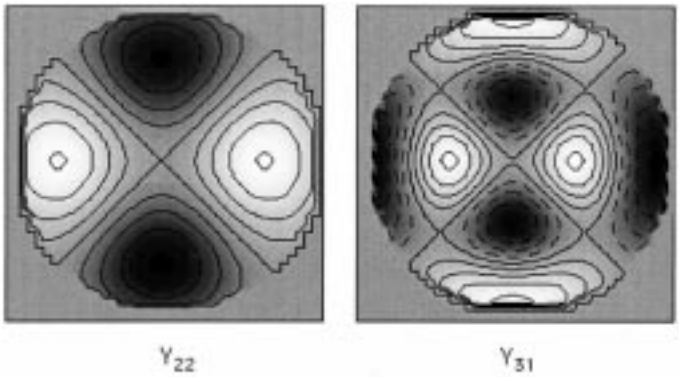

(a)

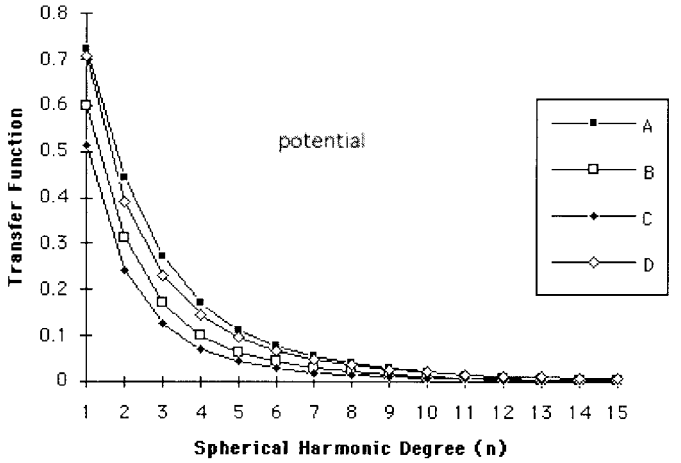

(b)

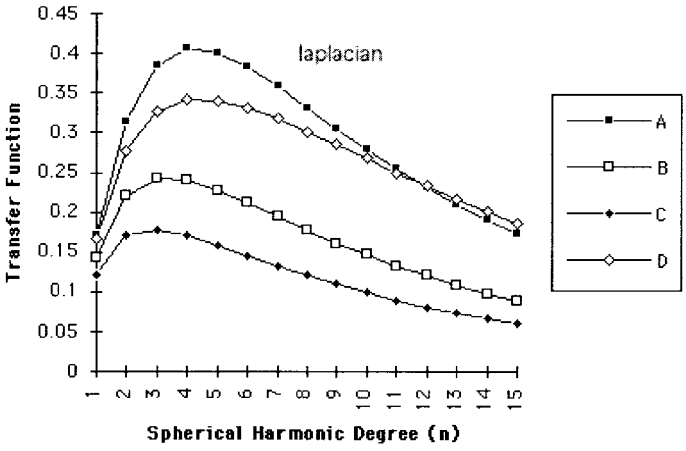

(c)

Fig. 1. (a) Examples of spherical harmonics $Y_{nm}(\theta, \phi)$: left, Y_{22} and right, Y_{31}. (b) Spatial transfer functions for scalp potential. Relative magnitude of each spatial frequency component (n). The four shells are at radii $(r_{\text{brain}}, r_{\text{CSF}}, r_{\text{skull}}, r_{\text{scalp}}) = (8, 8.2, 8.7, 9.2)$ cm. Cases A–C include a 2-mm CSF layer with $\sigma_{\text{BRAIN}}/\sigma_{\text{CSF}} = 0.2$ and D has no CSF layer. A: $\sigma_{\text{BRAIN}}/\sigma_{\text{SKULL}} = 40$. B: $\sigma_{\text{BRAIN}}/\sigma_{\text{SKULL}} = 80$. C: $\sigma_{\text{BRAIN}}/\sigma_{\text{SKULL}} = 120$. D: $\sigma_{\text{BRAIN}}/\sigma_{\text{SKULL}} = 80$. (c) Spatial transfer functions for scalp surface Laplacian. Relative magnitude of each spatial frequency component (n). The four shells are at radii $(r_{\text{brain}}, r_{\text{CSF}}, r_{\text{skull}}, r_{\text{scalp}}) = (8, 8.2, 8.7, 9.2)$ cm. Cases A–C include a 2-mm CSF layer with $\sigma_{\text{BRAIN}}/\sigma_{\text{CSF}} = 0.2$ and D has no CSF layer. A–D are the same as in (b).

Laplacian can be calculated analytically from the four spheres model [4]. The spatial transfer function for analytic surface

Laplacian is

$$T_{\mathrm{LAP}}(n) = n(n+1)\frac{4\pi}{2n+1}H_n. \tag{5}$$

The magnitude of this transfer function is plotted for different values of skull resistivity and CSF thickness in Fig. 1(c). By contrast to raw scalp potentials, the surface Laplacian has a bandpass spatial filtering characteristic. Estimates of the surface Laplacian from multichannel EEG recordings with a spline algorithm introduces low-pass spatial filtering in addition to that shown in Fig. 1(c), due to the application of smoothing filters to prevent aliasing from undersampled high spatial frequencies [4], [18].

III. Spatial Correlation by Volume Conduction

Spatial filtering by volume conduction alters coherence estimates by introducing artificial correlation between the recording channels. A quantitative estimate of this erroneous coherence is obtained here by modeling scalp potentials resulting from random neocortical sources with known statistics. Most spontaneous EEG is believed to be largely generated by superficial correlated dipole layers in neocortex [12] . In the four spheres model introduced in Section II, the EEG source distribution can be modeled as a random source field $B(r_Z, \theta, \phi, t)$ which produces the random scalp potential field $V_{\mathrm{SCALP}}(\theta, \phi, t)$. We can assume that the field has zero mean without loss of generality. The cross correlation function of the scalp potential (K_{SS}) can be calculated from the cross correlation of the source activity (K_{BB}) by

$$\begin{aligned} K_{SS}(\Omega_1, \Omega_2, t_1, t_2) = & \\ & \int_{S_1'}\int_{S_2'}\Big[G^*_{\mathrm{SCALP}}(\Omega_2, \Omega_2')K_{BB}(\Omega_1', \Omega_2', t_1, t_2) \\ & \cdot G_{\mathrm{SCALP}}(\Omega_1, \Omega_1')\,d\Omega_1'\,d\Omega_2'\Big]. \end{aligned} \tag{6}$$

Here, the compact notation $\Omega = (\theta, \phi)$ is introduced and the Green's function G_{SCALP} is given in (1). The form of this expression closely follows from the theory of random vibrations in structural dynamics [19]. If the excitation is weakly stationary, i.e.,

$$\begin{aligned} K_{BB}(\Omega_1, \Omega_2, t_1, t_2) &= K_{BB}(\Omega_1, \Omega_2, t_1 - t_2) \\ &= R(\Omega_1, \Omega_2, \tau) \end{aligned} \tag{7}$$

the scalp field is also weakly stationary and the cross spectral density of the scalp field is obtained by the Fourier transform

$$\begin{aligned} &\Phi_{SS}(\Omega_1, \Omega_2, \omega) \\ &\quad = \int_{S_1'}\int_{S_2'} G^*_{\mathrm{SCALP}}(\Omega_2, \Omega_2')\Phi_{BB}(\Omega_1', \Omega_2', \omega) \\ &\qquad \cdot G_{\mathrm{SCALP}}(\Omega_1, \Omega_1')\,d\Omega_1'\,d\Omega_2'. \end{aligned} \tag{8}$$

The cross spectral density of the scalp surface Laplacian can be derived by applying the Laplacian operator to the scalp potential Green's function. The cross spectral density function is the spatial correlation function between the two points Ω_1 and Ω_2 at the frequency ω. If $\Omega_1 = \Omega_2$ this reduces to the power spectral density function

$$F^2(\Omega, \omega) = \Phi(\Omega, \Omega, \omega). \tag{9}$$

If we normalize the cross spectral density function by the power spectral density functions at Ω_1 and Ω_2 (i.e., normalizing covariance by variances), we can define a frequency-dependent spatial correlation coefficient for raw scalp potential (S) and scalp Laplacian (L) which we identify as the usual coherence functions

$$\gamma^2_{SS}(\omega) = \frac{\Phi^2_{SS}(\Omega_1, \Omega_2, \omega)}{F^2_S(\Omega_1, \omega)F^2_S(\Omega_2, \omega)} \tag{10}$$

$$\gamma^2_{LL}(\omega) = \frac{\Phi^2_{LL}(\Omega_1, \Omega_2, \omega)}{F^2_L(\Omega_1, \omega)F^2_L(\Omega_2, \omega)}. \tag{11}$$

The coherence function is a squared correlation coefficient which depends on the pair of spatial locations Ω as well as the frequency ω.

The power spectral density function and the coherence function are estimated by forming a channel by channel cross spectral density matrix at each frequency, averaged over epochs to obtain a reliable estimate of the statistics of the underlying random process [1], [7]. The resultant estimates of cross spectral density between all possible pairs of channels in an EEG recording montage provides an estimate of the statistics of the spatio-temporal EEG process, filtered at the spatial frequencies that contribute to scalp samples for the particular recording strategy (reference, bipolar, or Laplacian). The filtering is a direct consequence of (6) and the spatial transfer functions shown here for scalp potentials and Laplacians in Fig. 1.

The effect of this spatial filtering on coherence estimates is easily demonstrated in the simplest case where the source activity is a spatially uncorrelated stationary random process

$$\Phi_{BB}(\Omega_1, \Omega_2, \omega) = \sigma^2(\omega)\delta(\cos\theta_1 - \cos\theta_2)\delta(\phi_1 - \phi_2). \tag{12}$$

Here, $\sigma^2(\omega)$ is the source variance as a function of frequency. Then the cross spectral density of the scalp potential is obtained by applying (1) and (8), yielding

$$\Phi_{SS}(\Omega_1, \Omega_2, \omega) = \sigma^2(\omega)\sum_{n-1}^{\infty}\frac{4\pi H_n^2}{2n+1}P_n(\cos\chi_{12}) \tag{13}$$

where χ_{12} is the angle between Ω_1 and Ω_2 and $P_n(x)$ are the Legendre polynomials. The power spectral density function is then

$$F^2_S(\omega) = \sigma^2(\omega)\sum_{n=1}^{\infty}\frac{4\pi H_n^2}{2n+1} \tag{14}$$

yielding the coherence function

$$\gamma^2_S(\chi_{12}, \omega) = \left[\frac{\displaystyle\sum_{n=1}^{\infty}\frac{H_n^2}{2n+1}P_n(\cos\chi_{12})}{\displaystyle\sum_{n=1}^{\infty}\frac{H_n^2}{2n+1}}\right]^2. \tag{15}$$

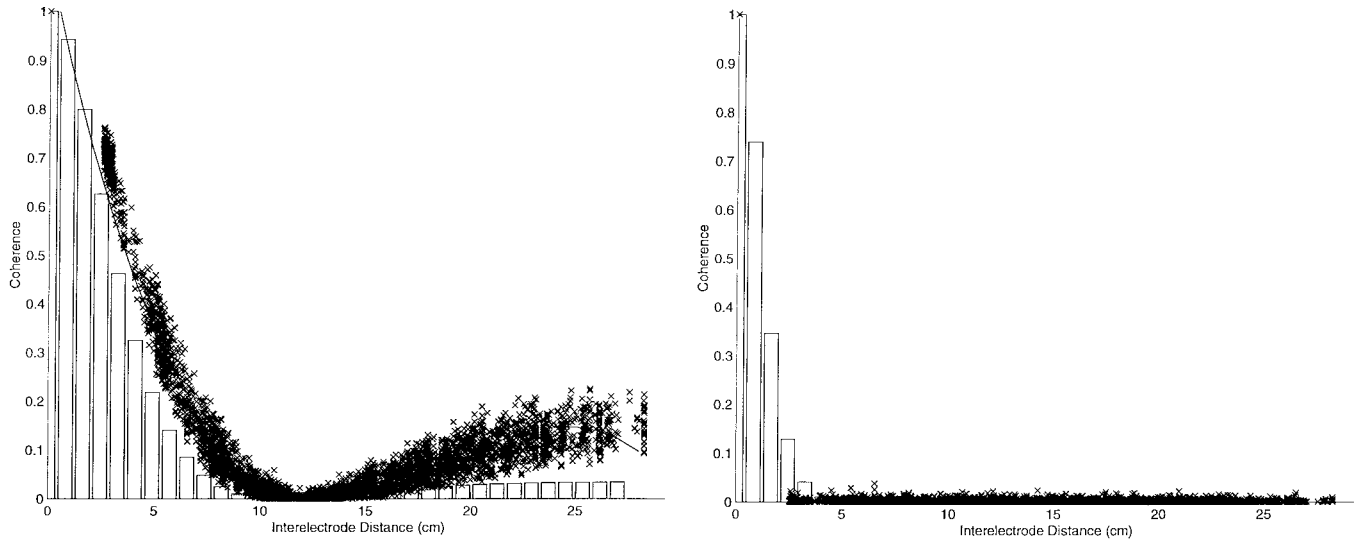

(a) (b)

Fig. 2. Coherence due to uncorrelated sources. (a) Reference-independent scalp potentials. (b) Analytic surface Laplacians. The analytic solutions for a superficial layer ($r_z = 7.8$) of uncorrelated sources are shown by the bars. Coherences (squared correlation coefficients) for all pairs of 111 scalp electrodes across 500 random distributions of 4240 superficial sources are shown by the scatter. The four spheres parameters are set to $(r_{\rm brain}, r_{\rm CSF}, r_{\rm skull}, r_{\rm scalp}) = (8, 8.2, 8.7, 9.2)$ cm and conductivity ratios $\sigma_{\rm brain/CSF} = 0.2$, $\sigma_{\rm brain/skull} = 80$, and $\sigma_{\rm brain/scalp} = 1$.

Similarly, the Laplacian coherence estimate is obtained as

$$\gamma_L^2(\chi_{12}, \omega) = \left[\frac{\sum_{n=1}^{\infty} \frac{n(n+1)H_n^2}{2n+1} P_n(\cos\chi_{12})}{\sum_{n=1}^{\infty} \frac{n(n+1)H_n^2}{2n+1}} \right]^2. \quad (16)$$

These coherence functions are plotted as a function of separation angle χ_{12} (measured in centimeters assuming a 9.2-cm radius scalp) in Fig. 2 (bars). When the coherence of a random process depends only on the separation distance, the process is termed homogeneous, which is analogous to time stationarity. In this case, the power spectral density function has frequency dependence, but is independent of position on the scalp surface. The coherence function is independent of both frequency and absolute position on the scalp surface, depending only on the separation distance between sensors. While this example is obviously a poor description of most EEG data, the curves generated in Fig. 2 are useful as a baseline for interpreting the physiological significance of coherence estimates from scalp data. The implication is that over short to moderate interelectrode distances (<10 cm in the spherical model) we may expect a significant contribution of coherence due to volume conduction. By contrast, the surface Laplacian yields erroneous high coherences only over short distances (<4 cm). In both cases, the volume conductor contribution to coherence is independent of temporal frequency, since tissue resistivities are insensitive to frequency over the narrow frequency range of EEG.

This simple example of uncorrelated sources fails to account for the dependence of EEG coherence on either temporal frequency or electrode position, and the contribution of volume conduction to EEG coherence appears to be additive. It is critical to recognize that the underlying process is filtering, as expressed by (6). In general, the cross spectral density of neocortical sources (ϕ_{BB}) is inhomogeneous (i.e., dependent on position within the brain), reflecting the spatial specificity of sources of neocortical rhythms [7], [12]. Thus, large correlated dipole layers (mostly low spatial frequency components) will make large contributions to coherence estimates based on scalp potentials, while smaller dipole layers (composed of higher spatial frequency components) will make larger contributions to Laplacian coherence estimates. This can result in higher coherences between electrode pairs in either Laplacian or potential data depending on the spatial bandwidth of the coherent activity. For example, suppose that EEG is due to a mixture of correlated and uncorrelated neocortical sources, and that the correlated sources at one temporal frequency are distributed as shown by the two spherical harmonics shown in Fig. 1(a). In a hypothetical experiment, we spatially narrow band filter the scalp data to a single spherical harmonic degree (n), for $n = 2$ and 3. Two electrodes that sit above any two peaks of Y_{21} will record a large coherence for the filter set at $n = 2$, but low coherence for the filter set to $n = 3$, as the electrodes are close to nodal lines of Y_{31}. The spatial filtering of raw potential and Laplacian shown in Fig. 1(b) and (c) indicates that the coherences recorded with each method are sensitive to distinct but partially overlapping spatial wavelengths. The relative magnitude of coherence with each method will depend on the spatial frequencies of the coherent neocortical sources.

IV. Simulations of Spatially Sampled EEG

The analytic solutions presented in Fig. 2 (bars) were based on reference-independent potentials, which are not available in EEG recordings. Every EEG electrode is referenced to another electrode typically placed on the head, chest, or neck. The neck reference is the effective reference for any choice of reference below the head [7]. This is a consequence of the fact that very little current flows below the neck. Thus, reference

recording involves performing a difference operation between two points on the head volume conductor. In the idealized case of "reference with respect to infinity" the contribution of spherical harmonic components of the scalp potential is zero for electrodes placed on the nodal lines of the harmonic functions. The reference recording shifts the location of the nodal lines, depending on the choice of reference. In the realistic case of irregular head geometry and inhomogeneous or anisotropic tissue properties, the transformation of the potential distribution by choice of reference will have a more complicated effect on the recorded potential.

Direct calculation of coherence on referenced potentials is compromised by the addition of the signal at the reference site to each of the electrodes [20], [21]. The relative power and phase angle between recording electrode and reference electrode will modify the spatial distribution of the signal and, consequently, the coherence estimates. One approach is to reference to the mathematical average of the mastoids or ears, which we can expect to bias coherences between channels close to these sites. Another approach is to employ the average reference, i.e., to estimate the instantaneous average potential and to subtract this quantity from each channel. In the ideal case of reference-independent sampling on a closed surface, such as a sphere, the dc signal is zero [22]. If the number of samples is sufficiently large and the head surface is completely sampled, the average reference simply removes the dc component of the spatial signal, which is entirely due to the reference electrode. However, if the spatial extent or number of electrodes is too small, new biases will be introduced by forcing a zero mean on the spatial signal. Another approach, more common in clinical studies, is to form close bipolar pairs which estimate local scalp tangential current density, but are difficult to interpret spatially because the potentials depend on the orientation of the bipolar pairs [4].

In order to simulate a spatially sampled EEG recording, 4240 random dipole sources were distributed in a layer covering the extent of the recording array (105° of elevation from vertex) within the inner sphere (brain) of the four spheres model at a fixed depth ($r_z = 7.8$ cm), with the model parameters set as in the analytic solution. Scalp potentials due to 500 different random source distributions (drawn from a uniform distribution) were then calculated from this model. Correlation coefficients were obtained between all possible pairs of 111 electrode positions (identical to those used in the EEG data discussed in a following section). Correlation coefficient squared was examined to allow direct comparison with the analytic coherence results.

Fig. 2 shows the coherence between all possible pairs of electrodes (6105) plotted against the analytic coherence results for reference-independent potentials and analytically calculated Laplacians. The analytic estimate is lower than the sampled estimate for the potentials because the effective number of sources used in the analytic calculation is infinite. As the number of sources is increased in the simulation, the two estimates converge. Both solutions show a small rise at long distances because the field of each dipole source falls off to zero with distance, but then rises again with opposite sign. In the case of the Laplacian, the sampling density was insufficient to verify the shape of the coherence function, but the nearest neighbor coherences are negligible in both the simulation and the analytic solution.

Fig. 3 shows the simulated coherence due to uncorrelated sources with (a) the average reference and (b) the average mastoids reference, for all possible pairs of electrodes. None (out of 6105) of the average reference coherences are shifted by more than 0.1 from the reference-independent case. In the case of the average mastoids reference, 2153 coherences change by 0.1 or more; at short distances ($<$15 cm) the effect is mostly to inflate coherences, while at longer distances the effect is mostly to reduce coherences, except for a small number of interhemispheric coherences (36) that increase due to proximity to the reference sites. By restricting the coherence pairs to a single hemisphere (51 electrodes), only 194 (out of 1225) average mastoids coherences change by more than 0.1 as shown in Fig. 3(c). In each plot referenced and reference-independent coherences are compared; coherences that change by less than 0.1 are indicated by a point, while coherences that change by more than 0.1 are indicated by an open circle. We do not suggest that a shift of 0.1 is necessarily the threshold for significance; in general confidence intervals for coherence estimates depend on both the number of epochs used and the coherence value [1], with larger coherence values having narrower confidence intervals. We use this criterion only to facilitate visualizing changes in the coherence function with reference electrode.

The spline-Laplacian is an estimate of the analytic surface Laplacian based on fitting either a spherical or three-dimensional (3-D) spline to instantaneous scalp potentials and calculating the second derivatives in the two surface coordinates [4], [15]–[18] Our study was based on 3-D splines which have a bandpass filtering characteristic to prevent aliasing from undersampled higher spatial frequencies [4]. Spline-Laplacian estimates were obtained at the 111 electrode locations and correlation coefficients calculated, demonstrating almost complete removal of volume conducted coherence artifact, as shown in Fig. 3(d). A small number of electrode pairs (16), show some inflated coherence particularly at the shortest distance corresponding to nearest neighbors. These electrode pairs all involved electrodes at the edge of the array, which are not constrained in the derivative estimates. As a consequence we have removed these coherences (153) in the analysis of the experimental Laplacian data.

These results suggest that the 3-D spline does not (in this simulation) introduce any erroneous high coherence, due only to the spline algorithm an effect that was reported in another study [23]. The most important difference between these two studies is that our study used a model of the head to generate realistic volume-conducted coherence. By contrast, in the earlier study the artificial correlation between electrodes was generated in simulations where spatial white noise was added to the raw signal prior to the Laplacian estimate. This was done by adding uncorrelated time series of random numbers to each electrode which is a spatial signal containing very high spatial frequencies. This approach might be appropriate for modeling the effects of amplifier or electrode noise, but not for sources in the brain. The influence of volume conduction is not simply the

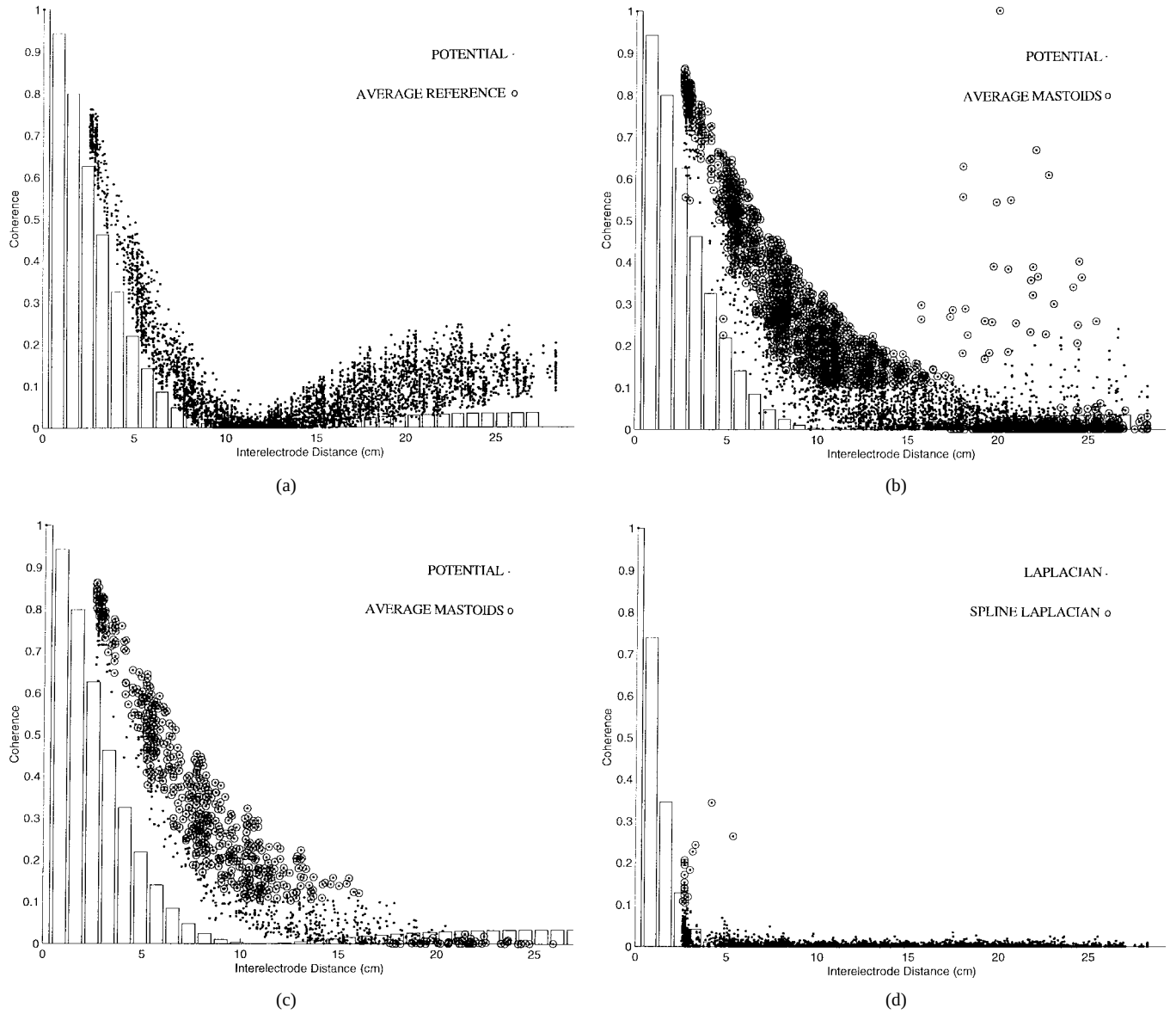

Fig. 3. Simulations of reference electrode and spline-Laplacian coherence due to uncorrelated sources: (a) average reference, (b) average mastoids (all channels) reference, (c) average mastoids (right hemisphere), and (d) spline-Laplacian. Coherences (squared correlation coefficients) for all possible pairs of 111 scalp electrodes are calculated from 500 random distributions of 4240 superficial ($r_z = 7.8$) sources. The four spheres parameters are set to $(r_{\rm brain}, r_{\rm CSF}, r_{\rm skull}, r_{\rm scalp}) = (8, 8.2, 8.7, 9.2)$ cm and conductivity ratios $\sigma_{\rm brain/CSF} = 0.2$, $\sigma_{\rm brain/skull} = 80$, and $\sigma_{\rm brain/scalp} = 1$. In plots (a)–(c) coherences that are within 0.1 of the simulation of reference-independent potentials are shown with a point; coherences that change by more than 0.1 are shown with an open circle. In plot (d) coherences that are within 0.1 of the simulation of analytic Laplacian coherence are shown with a point; coherences that change by more than 0.1 are shown with an open circle.

addition of noise to the data, but rather spatial filtering of the data which has the effect of artificially correlating electrodes when the neocortical sources are uncorrelated. There may also be small differences due to the high-pass characteristic of spherical splines used in the earlier study in contrast to the bandpass characteristic of 3-D splines used in this study. This can be easily corrected as spherical spline algorithms can be smoothed to produce a bandpass characteristic [18]. However, we have not made any direct comparisons between the 3-D and spherical splines. The 3-D spline Laplacian has also been tested by estimating local spline Laplacians for the major scalp regions centered approximately at P3, P4, F3, and F4, from independent sets of 12 channels [12]. The six pairs of coherence spectra obtained in this manner were compared to the same pairs from the global spline Laplacian estimate. The spectra were largely consistent between the two estimates. The only significant difference occurred for the pair F3 : F4 where the coherence was found to be lower in the global spline Laplacian. Thus, we have confidence that our Laplacian estimate does not introduce algorithmic coherence artifacts.

V. Spontaneous EEG Coherence

The EEG data presented here were recorded from one female adult subject (20 yrs) using a 129-channel geodesic sensor net [24], providing a mean interelectrode distance of 2.7 cm, subtending an angle of 120° from vertex. We have examined the records of 31 adults subjects (18–24 yrs old) and

describe only general patterns of EEG coherence common to the subjects. Two minutes of eyes-closed and eyes-open EEG were recorded in this "resting" state. A vertex reference was used and the records were digitized at 200 Hz with the low-pass analog filter set to 50 Hz. In order to avoid influencing the results of dynamical analysis by artifact, all time series were visually inspected for standard artifacts such as eye blinks and muscle activity. Furthermore, automated rejection of possible artifact was accomplished using amplitude criteria. Eighteen data channels on the outer most ring of electrodes on the inferior surface of the head were dropped from the study due to possible artifacts, leaving 111 electrode sites. Average referenced data was obtained by re-referencing the vertex referenced potentials to the instantaneous average potential of all 111 channels. Average mastoids referenced data was obtained by re-referencing the data to the mathematical average of the two mastoid electrodes. The electrode positions were fit to a sphere and all distances reported are along this sphere. The data were used to fit a 3-D spline at each time point and the Laplacian estimate was obtained. The data were divided into 2-s epochs and Fourier transformed (using MATLAB) obtaining a 0.5-Hz frequency resolution to calculate the coherences between all pairs (6105) of channels. The 95% confidence intervals for coherence depend on both the number of epochs and the coherence value; for the 60 epochs used here a high coherence of 0.8 has a confidence interval [0.7 0.9], while a small coherence of 0.2 has a confidence interval [0.1 0.6] [1], [24].

At each frequency, the coherence data showed different contributions from coherent sources, reference electrode, and volume conduction. From the analytic solution, (15), we expect that the contribution of volume conduction of uncorrelated sources will be independent of frequency [7], [12]. Fig. 4 shows EEG coherence as a function of frequency in the eyes-closed condition between electrode Oz and a succession of electrodes (separated by 2.57 cm) along the midline in the anterior direction. The coherence between Oz and the electrodes 68, Pz, and 55, clearly indicate a strong component of volume conduction as the coherence is relatively independent of frequency with both the average reference and average mastoids reference. The Oz : Cz pair (10.28-cm separation) shows peaks in the coherence spectrum with both references. All four coherence pairs show higher coherences in the average mastoids reference than the average reference, consistent with the simulations at these distances (Fig. 3). The pair Oz : Fz shows differences between average reference and average mastoids coherence that are specific to the 8–32 Hz range; they are probably due to differences in the spatial distributions of frequency components in relation to reference locations.

By contrast, the surface Laplacian data shows significant coherence that is independent of frequency only for the first pair (Oz : 68). The Laplacian coherence becomes negligible at frequencies above 25 Hz at Oz : Pz (separated by 5.14 cm) and for electrode pairs at greater distances. By contrast, the two reference potential coherence measurements have large magnitude, but are relatively frequency independent. At lower frequencies, such as the alpha band (8–12 Hz), electrode pair specific coherences are seen in the Laplacian data in comparison to the rest of the spectrum. For instance, a clear peak can be seen at 10 Hz at a distance of 5.14 cm (Oz : Pz) and at a distance of 10.28 cm (Oz : Cz), that is absent in Oz : 55 at the intermediate distance of 7.71 cm. Apparently, in this subject this electrode (55) sits close to a nodal line of the pattern of alpha sources close to 10 Hz filtered at the spatial wavelengths of Laplacian data. This nodal line is apparently quite distinct from nodal lines of the adjacent alpha frequencies, 9.5 and 10.5 Hz.

We directly compared the coherence as a function of inter-electrode distance between a low EEG frequency (10 Hz) and a high EEG frequency (38 Hz) with each reference potential and the Laplacian in both eyes-closed and eyes-open conditions. Fig. 5 shows the coherence scatter for 51 right-hemisphere electrodes (1225 pairs) in the eyes-closed condition; qualitatively similar plots were obtained for the left hemisphere and in both hemispheres in the eyes-open condition. We examined these restricted sets because the average mastoid reference strongly influences interhemispheric coherences as shown in Fig. 3. With both the average reference [Fig. 3(a)] and the average mastoids reference [Fig. 3(b)] high coherences are shown at 10 Hz at long interelectrode distances ($>$15 cm), which are somewhat higher in the average reference case in contrast to very few high coherences shown at 38 Hz. At both frequencies, the shift in long-range coherence between average reference and average mastoids is comparable in magnitude to the simulations with uncorrelated sources (Fig. 3). In all plots a polynomial fit to the coherence distance function is shown. At 10 Hz, the coherence function shows a trend to a minimum is at intermediate distances ($\sim$14 cm) before rising again at long distances. At all distances the 10-Hz coherences are generally higher than the 38-Hz coherences. Since the electrode pairs were restricted to a hemisphere, all of the long-range coherences shown here are oriented in anterior–posterior directions. The pattern of referenced potential coherence at 10 Hz matches a putative source distribution of very low spatial wavelength, possibly comprised of two broad correlated dipole layers under posterior and anterior electrodes, which tend to oscillate 180° out of phase in the manner of a standing wave [12].

The coherences at 38 Hz seem to mostly fall off regularly with distance suggesting they are mostly due to volume conduction. This is supported by the Laplacian coherences at 38 Hz [Fig. 5(c)] which are mostly negligible at distances greater than 5 cm. By contrast, a large number of high coherences are shown between 5 and 20 cm at 10 Hz, but at long distances ($>$20 cm) the coherences are mostly reduced in comparison to the referenced potential data. This suggests that while the Laplacian is able to detect the genuine coherences at short and intermediate (5–20 cm) interelectrode distances with better resolution than the potential (because of its spatial bandpass characteristic), the attenuation of low-spatial frequencies by the Laplacian reduces some genuine long-range coherences generated by neocortical dynamics [12].

The changes in coherence when switching between the two references and the Laplacian could (in part) be predicted by the simulations. Table I shows the number of coherences that changed by at least 0.1 (in either direction) in changing

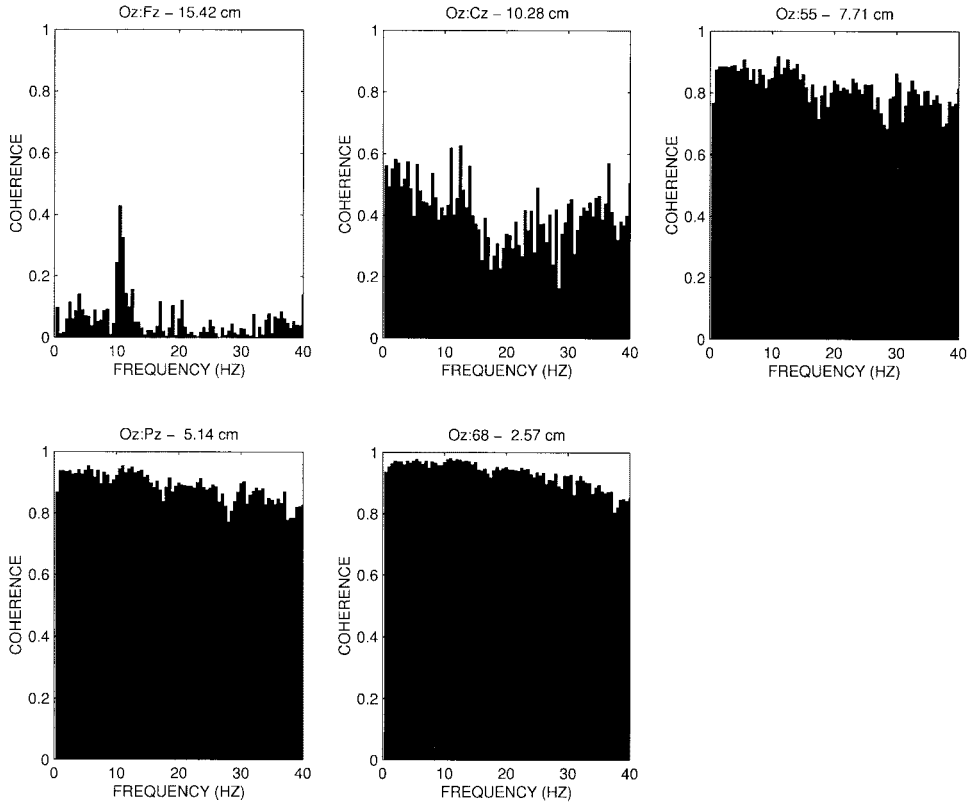

(a)

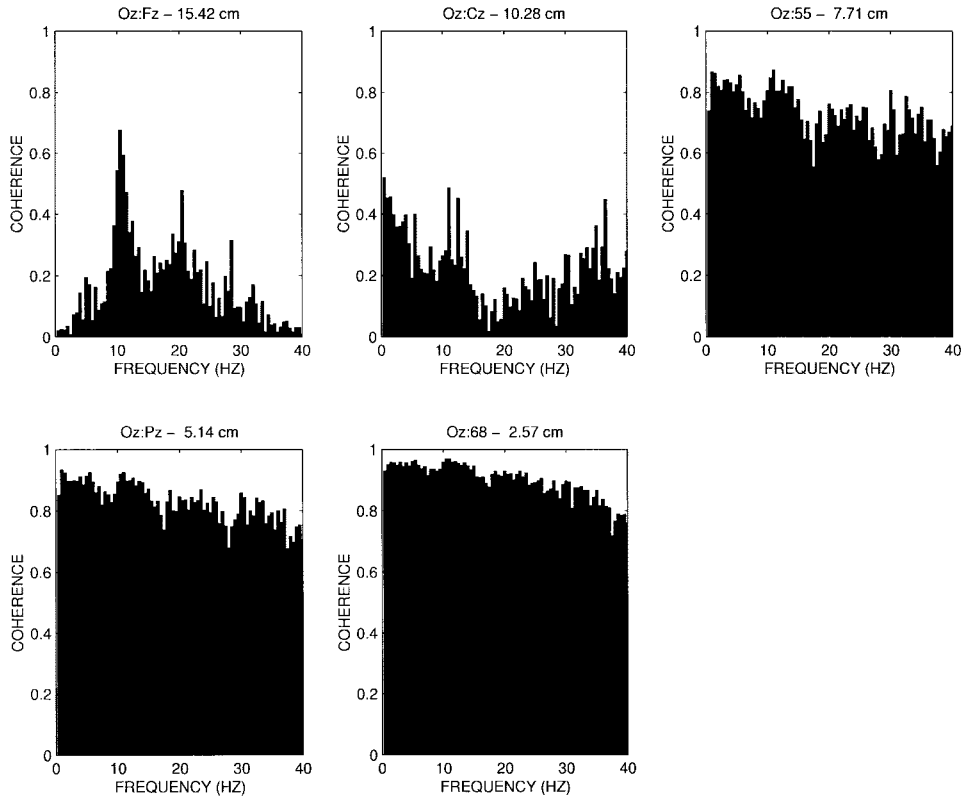

(b)

Fig. 4. Coherence spectra in the posterior–anterior direction along the midline with respect to electrode Oz: (a) average mastoids reference and (b) average reference. Data shown is from one subject in the eyes-closed resting condition. Coherence was estimated from 60 2-s epochs (0.5-Hz frequency resolution). The channel names correspond to the 10–20 system for some of the electrodes; electrodes in between the 10–20 electrodes are identified by number. The reported interelectrode distances are along a best-fit sphere to the electrode positions.

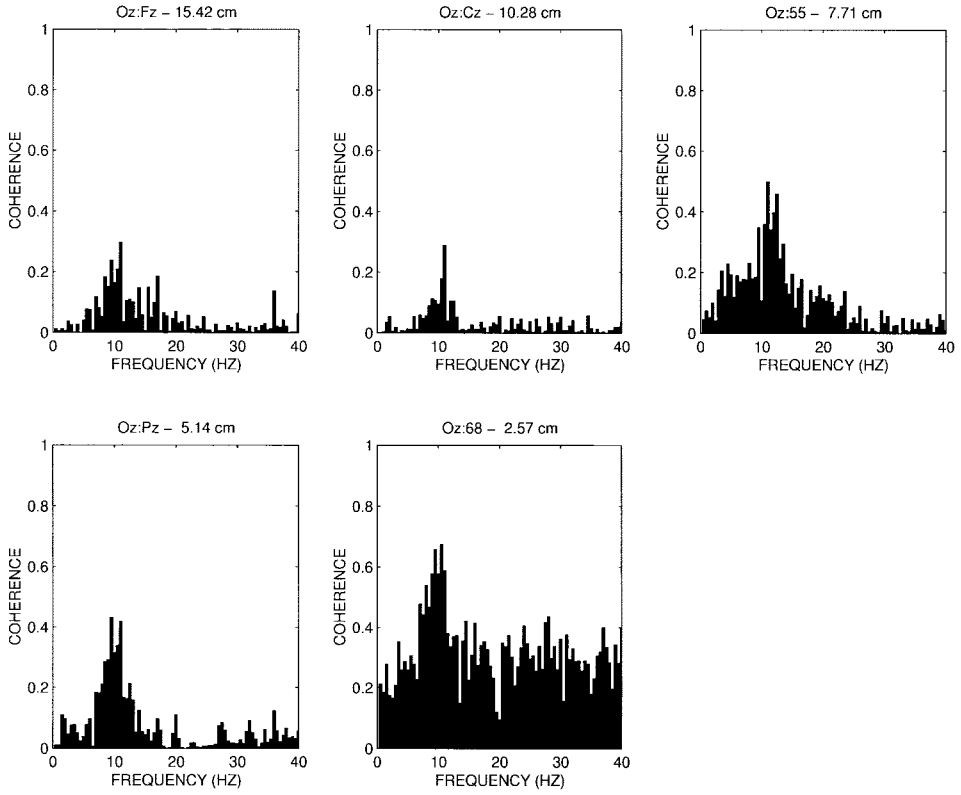

(c)

Fig. 4. (*Continued*.) Coherence spectra in the posterior–anterior direction along the midline with respect to electrode Oz: (c) surface Laplacian. Data shown is from one subject in the eyes-closed resting condition. Coherence was estimated from 60 2-s epochs (0.5-Hz frequency resolution). The channel names correspond to the 10–20 system for some of the electrodes; electrodes in between the 10–20 electrodes are identified by number. The reported interelectrode distances are along a best-fit sphere to the electrode positions.

between references in the simulations and EEG data. For each entry the number in the parenthesis indicates the number of coherences that increased by at least 0.1. The numbers are shown combining the left and right hemisphere results from a total of 2250 coherences. In the simulation average mastoids has higher coherences than average reference except for approximately 100 long-range coherences. The Laplacian reduces coherences due to volume conduction and reference with no coherences increasing. In the EEG data, at both frequencies and in both eyes-closed and eyes-open conditions, the difference between mastoids and average reference coherence was not mostly positive as in the simulations. This discrepancy may have occurred because each of the experimental conditions probably included some correlated sources near the mastoids and/or deeper sources that differentially influence other electrodes, depending on the relative phase of each channel with respect to the average of the mastoids [20]. This suggests that neither reference provides a perfect picture of the potential coherence, but at long distances both are useful, with the average mastoids being more suitable for intrahemispheric coherences at long distances as it cancels some of the volume conduction effects. In the comparison between Laplacian and mastoids or average reference, a striking difference is noted between the experimental 10-Hz and 38-Hz results and simulations. The 38-Hz response is similar to the simulation with most coherences lower using the Laplacian. However, at 10 Hz approximately 30% of the Laplacian coherences are larger; these occur mostly at interelectrode distances between 5 and 20 cm. This implies that 10-Hz coherent source distributions exist in the data filtered by both the referenced potential and the Laplacian, while at 38 Hz most of the potential coherence was due to volume conduction of uncorrelated sources.

VI. Discussion

The spatial filtering inherent in both the scalp potential field and the surface Laplacian estimate of cortical potentials imply that each approach is sensitive to distinct, but partially overlapping spatial scales of the dynamics. Both the simulations and data examined here confirm this qualitative property of scalp recorded EEG. The simulations and analytic solutions predict that volume conduction of uncorrelated sources inflate coherence estimates for electrode pairs within 10–12 cm. This artificial correlation is reduced by the surface Laplacian estimate of cortical potentials. The analytic solution reveals that this process is not additive, but is spatial filtering, implying that the potential and Laplacian coherences are representations of source statistics at distinct spatial wavelengths. The EEG data was consistent with these predictions. At 10 Hz, distinct patterns of source correlations are observed in the referenced potential and Laplacian data, while at high frequencies (38 Hz) most of the referenced potential coherences are due to volume conduction, which are reduced substantially by the Laplacian.

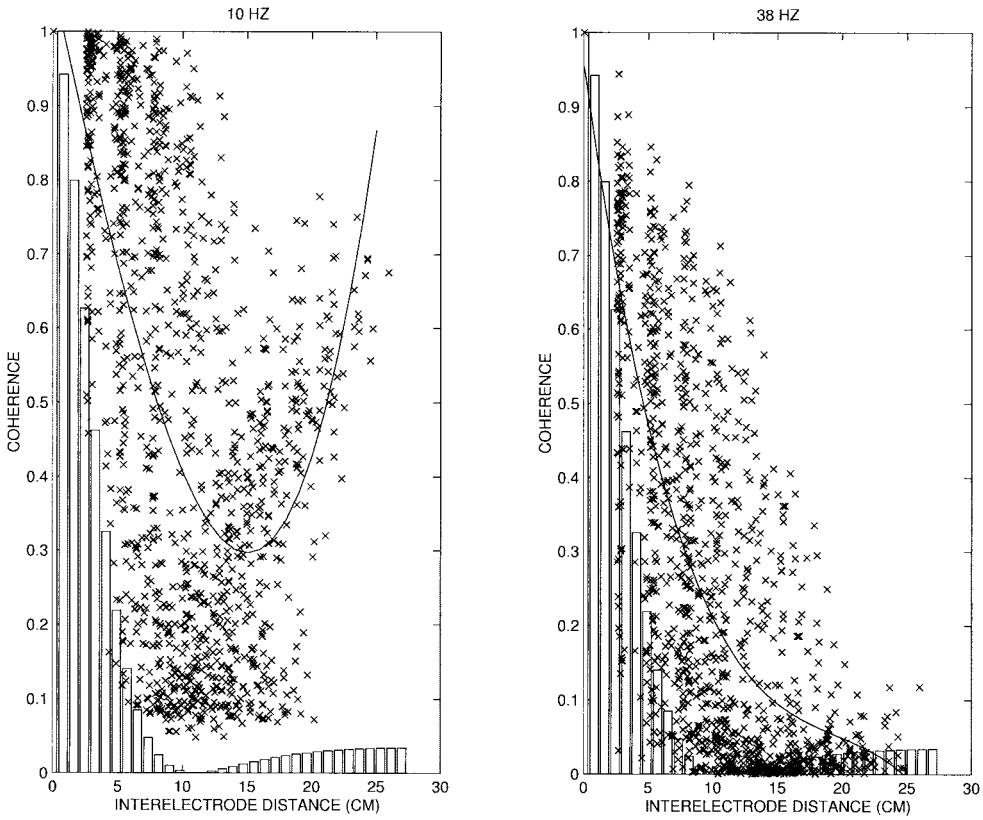

(a)

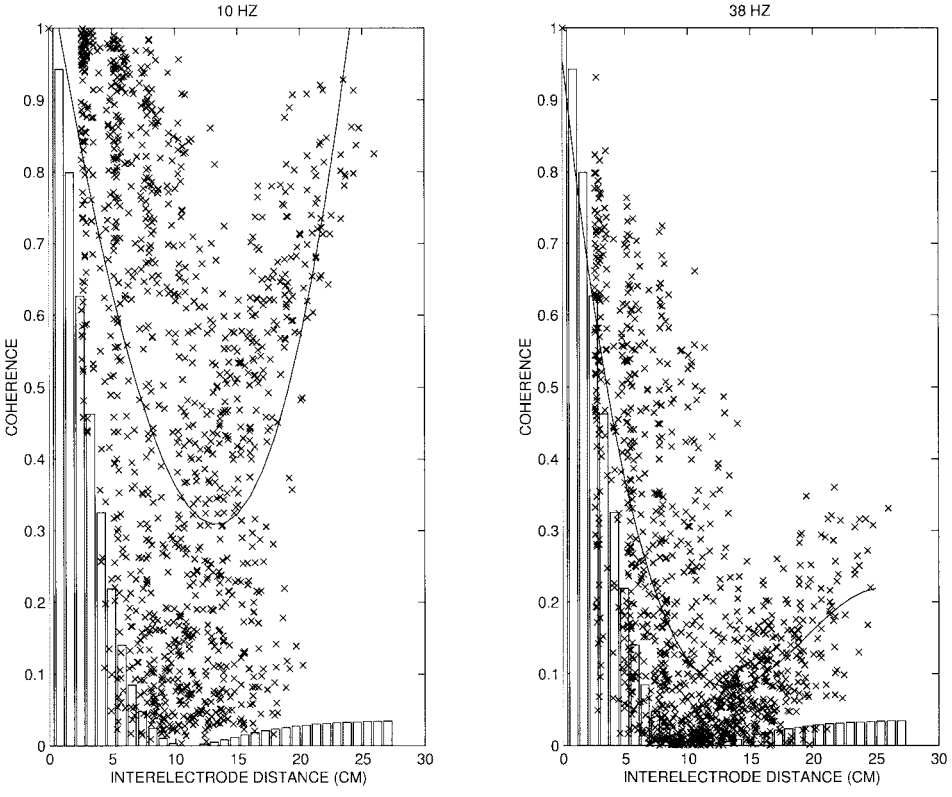

(b)

Fig. 5. Scatter of all coherence pairs versus interelectrode distance among right-hemisphere electrodes (51) at (left) 10 Hz and (right) 38 Hz. (a) Average mastoids reference and (b) average reference. Third-order polynomial fits to the coherence scatter are plotted. The analytic coherence estimate for uncorrelated sources is shown by the bars.

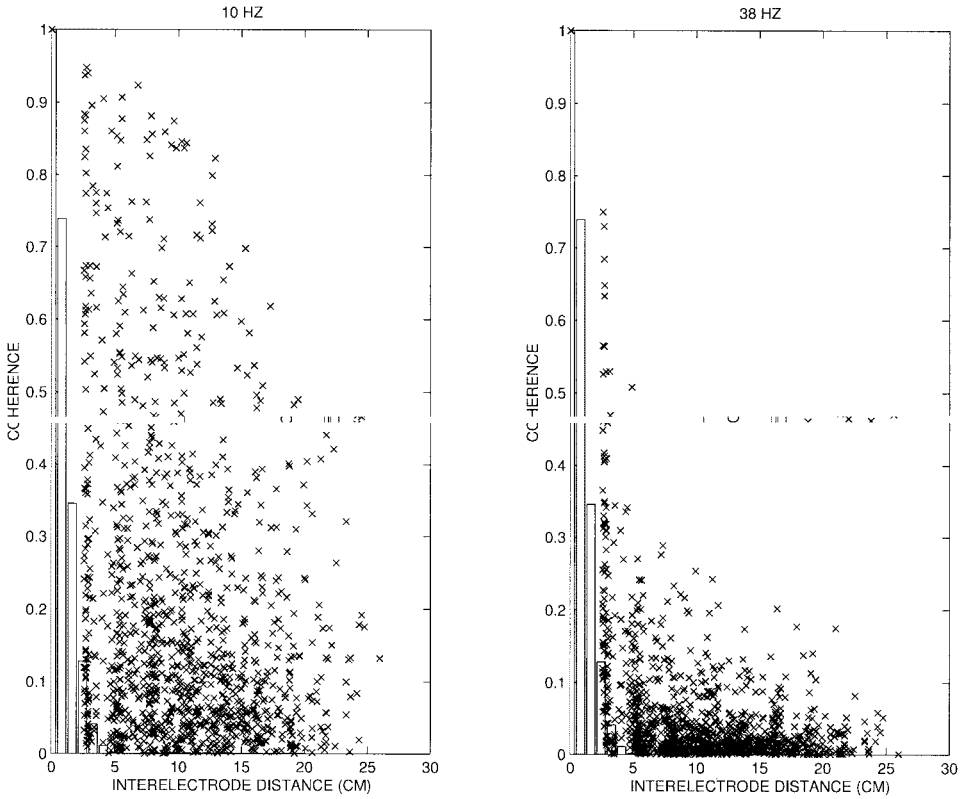

(c)

Fig. 5. (*Continued*.) Scatter of all coherence pairs versus interelectrode distance among right-hemisphere electrodes (51) at (left) 10 Hz and (right) 38 Hz. (c) Spline-Laplacian. Third-order polynomial fits to the coherence scatter are plotted. The analytic coherence estimate for uncorrelated sources is shown by the bars.

TABLE I
CHANGES IN COHERENCE ESTIMATES WITH CHANGES IN REFERENCE. EACH ROW IS THE COMPARISON BETWEEN REFERENCED POTENIALS OF LAPLACIAN FOR THE TWO FREQUENCIES (10 AND 38 Hz) IN THE TWO CONDITIONS (EYES CLOSED AND EYES OPEN)

Comparison	simulation	10 Hz eyes closed	10 Hz eyes open	38 Hz eyes closed	38 Hz eyes open
mastoid–average	1054 (956)	552 (224)	620 (296)	546 (56)	434 (220)
Laplacian–average	878 (0)	1814 (501)	1554 (469)	1112 (114)	1094 (188)
Laplacian–mastoid	1356 (0)	1786 (498)	1542 (441)	978 (97)	1086 (86)

Entries are the number of coherences that changed by at least 0.1. The numbers in parentheses are the number of these coherences that increased by at least 0.1, i.e., a positive difference between the first method and the second. All of the numbers were taken from simulations or 2-min EEG records from one subject, with 0.5-Hz frequency resolution. Coherences were computed between electrode pairs in the same hemisphere using 51 electrodes over each hemisphere, for a total of 2250 coherences.

Many experimental papers on EEG coherence have avoided the issue of volume conduction. A common misconception is that volume conduction is additive and can, thus, be ignored in the comparison of two or more conditions in the same subject or between groups of subjects [26], [27]. The theoretical developments in this paper suggest that the effectiveness of the comparisons are compromised by this assumption in two ways: 1) The inflation of coherence estimates at short distances by volume conduction of uncorrelated sources biases statistical analysis of task condition or group differences. Changes in weak correlation at short distances can appear highly significant as the confidence intervals on coherence values are narrower for higher coherence values. 2) Only changes of source correlation at very low spatial frequencies (i.e., large dipole layers) are robust in raw potential data. Correlations between smaller dipole layers are relatively attenuated in the raw potential data, so that statistical significance of changes in coherence is reduced.

The surface Laplacian approach improved the resolution of these intermediate length coherences due to its bandpass spatial filtering characteristic. In the simulations using uncorrelated sources, the surface Laplacian algorithm removed all of the coherences due to volume conduction for 111 electrodes. In the case of high-frequency data (38 Hz), most of the coherences were reduced by the surface Laplacian, suggesting that they were largely due to volume conduction. But in the alpha frequency data (10 Hz) many of the coherences at intermediate lengths (5–20 cm) increased. This suggests that at 10 Hz, short and intermediate wavelengths of correlated sources exists along with robust long-range coherences ($>$20 cm). These

long-range coherences were reduced in the surface Laplacian estimate because its spatial bandpass characteristic attenuates low spatial frequencies. Thus, the surface Laplacians do not replace the referenced potentials, but rather should be used in parallel to improve the information yield in studies of EEG coherence.

By contrast to the relatively high coherences at electrode separations greater than 5 cm, intracranial coherences are normally much smaller at comparable distances. For example, subdural coherence measured with 2-mm-diameter electrodes typically falls to zero at all frequencies at electrode separations greater than about 2 cm [28]. Apparently, large- and intermediate-scale recordings from scalp electrodes of 1-cm diameter provide recordings at a distinct spatial scale of EEG dynamics. Nearly all physiologically based models of dynamic interactions of neurons in neocortex suggest spatial-temporal dynamic behaviors with preferred ranges in both spatial (k) and temporal (ω) frequencies for the spectral density function $S(k,\omega)$. These include local neural circuits with local negative and positive feedback [29], [30], global theory that includes delays of signals transmitted along corticocortical fibers [12], [31], [32], combined local/global theory [12], [33], and statistical mechanics of neocortical interactions [34]. The global theory predicts multiple spatial frequencies (k) contributing over the same range of temporal frequencies (ω) even in linear limiting cases [12], [32]. Thus, neocortical dynamic processes can, themselves, be expected to act as a spatio–temporal filter on cortical inputs. Scalp recording involves further spatial filtering of this response function due to volume conduction. Differences between cortical and scalp temporal frequency spectra [35] apparently occur as an indirect result of this spatial filtering.

Despite some simplifying assumptions, the theory and simulations outlined here provide a useful guide to interpreting experimental coherence studies. The filtering properties of the head equation (6) depend on the head model and depth of source distribution; we have used a superficial radial dipole layer in a four spheres model. However, the general form of the filter, and the simulation techniques, are equally applicable to spatial correlations among tangential dipole sources, and should provide qualitatively similar results. Further improvements to the modeling could be achieved by the use of a realistic finite-element model. In this case, the analytic approach is not possible, but realistic simulations of coherence due to uncorrelated sources could provide a more precise aid in the interpretation of EEG data.

APPENDIX
THE FOUR CONCENTRIC SPHERES MODEL OF THE HEAD

For a radial dipole, the solution to the four spheres model is expressed in each sphere i [$i = 1$ (brain), 2 (CSF), 3 (skull), and 4 (scalp)] as

$$V_i(r,\theta,\psi) = \sum_{n=0}^{\infty}\left[A_n^i\left(\frac{r}{r_i}\right)^n + B_n^i\left(\frac{r_i}{r}\right)^{n+1}\right]P_n(\cos\theta) \tag{A-1}$$

where P_n are the Legendre polynomials and boundary conditions are applied to obtain the solutions as a set of recursion relations for the coefficients. The solution for tangential dipoles is of the same form but with the sums over the associated Legendre polynomials. The terms corresponding to $n = 0$ have zero contribution as a consequence of current conservation.

We introduce the notation $r_{ij} = r_i/r_j$ and $\sigma_{ij} = \sigma_i/\sigma_j$ to indicate the radii and conductivity ratios between the model layers. For convenience we define the quantities

$$V_n = \frac{\sigma_{34}\dfrac{n+1}{n} - \dfrac{r_{34}^n - r_{43}^{n+1}}{\dfrac{n+1}{n}r_{34}^n + r_{43}^{n+1}}}{\sigma_{34} + \dfrac{r_{34}^n - r_{43}^{n+1}}{\dfrac{n+1}{n}r_{34}^n + r_{43}^{n+1}}} \tag{A-2}$$

$$Y_n = \frac{\sigma_{23}\dfrac{n}{n+1} - r_{23}^n\dfrac{\dfrac{n}{n+1} - V_n r_{32}^{n+1}}{r_{23}^n + V_n r_{32}^{n+1}}}{\sigma_{23} + \dfrac{r_{23}^n\dfrac{n}{n+1} - V_n r_{32}^{n+1}}{r_{23}^n + V_n r_{32}^{n+1}}} \tag{A-3}$$

$$Z_n = \frac{r_{12}^n - \dfrac{n+1}{n}Y_n r_{21}^{n+1}}{r_{12}^n + Y_n r_{21}^{n+1}}. \tag{A-4}$$

Then the model coefficients are

$$A_n^1 = \frac{r_{z\boldsymbol{l}}^{n-1}[nZ_n + \sigma_{12}(n+1)]}{4\pi r_1^2(\sigma_{12} - Z_n)} \tag{A-5}$$

$$A_n^2 = \frac{A_n^1 + \dfrac{n r_{z1}^{n-1}}{4\pi r_1^2}}{Y_n r_{21}^{n+1} + r_{12}^n} \tag{A-6}$$

$$B_n^2 = A_n^2 Y_n \tag{A-7}$$

$$A_n^3 = \frac{A_n^3 + B_n^2}{r_{23}^n + V_n r_{32}^{n+1}} \tag{A-8}$$

$$B_n^3 = V_n A_n^3 \tag{A-9}$$

$$A_n^4 = \frac{n+1}{n}\left(\frac{A_n^3 + B_n^3}{\dfrac{n+1}{n}r_{34}^n + r_{43}^{n+1}}\right) \tag{A-10}$$

$$B_n^4 = A_n^4\frac{n}{n+1}. \tag{A-11}$$

The scalp surface potential $V_S(\theta,\phi)$ is calculated as

$$V_S(\theta,\phi) = \sum_{n=1}^{\infty} H_n P_n(\cos\theta) = \sum_{n=1}^{\infty}(A_n^4 + B_n^4)P_n(\cos\theta). \tag{A-12}$$

REFERENCES

[1] J. S. Bendat and A. Piersol, *Random Data: Analysis and Measurement Procedures.* New York: Wiley, 1986.

[2] R. S. Hoesk, A. Sances, R. W. Jodat, and S. J. Larson, "The contribution of intracerebral currents to the EEG and evoked potentials," *IEEE Trans. Biomed. Eng.,* vol. 25, pp. 405–413, 1978.

[3] B. N. Cuffin and D. Cohen, "Comparison of the magnetoencephalogram and the electroencephalogram," *Electroencephalogr., Clin. Neurophysiol.,* vol. 47, pp. 136–146, 1979.

[4] R. Srinivasan, P. L. Nunez, D. M. Tucker, R. B. Silberstein, and P. J. Cadusch, "Spatial sampling and filtering of EEG with spline Laplacians to estimate cortical potential," *Brain Topogr.*, vol. 8, pp. 355–366, 1996.
[5] H. Zhou and A. van Oostrom, "Computation of the potential in a four layer anisotropic concentric spherical volume conductor," *IEEE Trans. Biomed. Eng.*, vol. 39, pp. 154–158, 1992.
[6] C. J. Stok, "The influence of model parameters on EEG/MEG single dipole source estimation," *IEEE Trans. Biomed. Eng.*, vol. BME-34, pp. 289–296, 1987.
[7] P. L. Nunez, *Electric Fields of the Brain: The Neurophysics of EEG.* New York: Oxford Univ. Press, 1981.
[8] S. K. Law, "Thickness and resistivity variations over the upper surface of the human skull," *Brain Topogr.*, vol. 6, pp. 99–110, 1993.
[9] Y. Yan, P. L. Nunez, and R. T. Hart, "A finite element model of the human head: Scalp potentials due to dipole sources," *Med., Biol. Eng., Comput.*, vol. 29, pp. 475–481, 1991.
[10] S. Rush and D. A. Driscoll, "EEG electrode sensitivity: An application of reciprocity," *IEEE Trans. Biomed. Eng.*, vol. BME-16, pp. 15–22, 1968.
[11] R. B. Silberstein and P. J. Cadusch, "Measurement processes and spatial principal components analysis," *Brain Topogr.*, vol. 4, pp. 267–276, 1992.
[12] P. L. Nunez, *Neocortical Dynamics and Human EEG Rhythms.* New York: Oxford Univ. Press, 1995.
[13] R. Freidrich, A. Fuchs, and H. Haken, "Spatiotemporal EEG patterns," *Rhythms in Physiological Systems*, H. Haken and H. P. Koepchen, Eds. Berlin, Germany: Springer-Verlag, 1991.
[14] R. B. Paranjape, Z. J. Koles, and J. Lind, "A spatial power spectrum analysis of the electroencephalogram," *Brain Topogr.*, vol. 3, pp. 329–356, 1993.
[15] P. L. Nunez, R. B. Silberstein, P. J. Cadusch, and R. S. Wijesinghe, "Comparison of high resolution methods having different theoretical bases," *Brain Topogr.*, vol. 5, pp. 361–364, 1993.
[16] P. L. Nunez, R. B. Silberstein, P. J. Cadusch, R. Wijesinghe, A. F. Westdorp, and R. Srinivasan, "A theoretical and experimental study of high resolution EEG based on surface Laplacians and cortical imaging," *Electroencephalogr., Clin. Neurophysiol.*, vol. 90, pp. 40–57, 1994.
[17] S. K. Law, P. L. Nunez, and R. S. Wijesinghe, "High-resolution EEG using spline generated surface Laplacians on spherical and ellipsoidal surfaces," *IEEE Trans. Biomed. Eng.*, vol. 40, pp. 145–152, 1993.
[18] F. Perrin, J. Pernier, O. Bertrand, and J. F. Echallier, "Spherical splines for scalp potential and current density mapping," *Electroencephalogr., Clin. Neurophysiol.*, vol. 72, pp. 184–187, 1989.
[19] Y. K. Lin, *Probabilistic Theory of Structural Dynamics.* New York: McGraw Hill, 1967.
[20] G. Fein, J. Raz, F. F. Brown, and E. L. Merrin, "Common reference coherence data are confounded by power and phase effects," *Electroencephalogr., Clin. Neurophysiol.*, vol. 72, pp. 581–584, 1988.
[21] J. C. de Munck, P. C. M. Vijn, and F. H. Lopes da Silva, "A random dipole model for spontaneous EEG," *IEEE Trans. Biomed. Eng.*, vol. 39, pp. 791–803, 1992.
[22] O. Bertrand, F. Perrin, and J. Pernier, "A theoretical justification of the average reference in topographic evoked potential studies," *Electroencephalogr., Clin. Neurophysiol.*, vol. 62, pp. 462–464, 1985.
[23] C. A. Biggins, G. Fein, J. Raz, and A. Amir, "Artifactually high coherences from using spherical spline computation of scalp current density," *Electroencephalogr., Clin. Neurophysiol.*, vol. 79, pp. 413–419, 1991.
[24] D. M. Tucker, "Spatial sampling of head electrical fields: The geodesic sensor net," *Electroencephalogr., Clin. Neurophysiol.*, vol. 87, pp. 154–163, 1993.
[25] P. L. Nunez, R. Srinivasan, A. F. Westdorp, R. S. Wijesinghe, D. M. Tucker, R. B. Silberstein, and P. J. Cadusch, "EEG coherency I: Statistics, reference electrode, volume conduction, Laplacians, cortical imaging, and interpretation at multiple scales," *Electroencephalogr., Clin. Neurophysiol.*, vol. 103, pp. 499–515, 1997.
[26] R. W. Thatcher, P. J. Krause, and M. Hrybyk, "Corticocortical associations and EEG coherence: A two compartment model," *Electroencephalogr., Clin. Neurophysiol.*, vol. 64, pp. 123–143, 1986.
[27] D. M. Tucker, D. L. Roth, and T. B. Bair, "Functional connections among cortical regions: Topography of EEG coherence," *Electroencephalogr., Clin. Neurophysiol.*, vol. 63, pp. 242–250, 1986.
[28] T. H. Bullock, M. C. McClune, J. Z. Achimowicz, V. J. Iragui-Madoz, R. B. Duckrow, and S. S. Spencer, "EEG coherence has structure in the millimeter domain: Subdural and hippocampal recordings from epileptic patients," *Electroencephalogr., Clin. Neurophysiol.*, vol. 95, pp. 161–177, 1995.
[29] A. van Rotterdam, F. H. Lopes da Silva, J. van den Ende, M. A. Viergever, and A. J. Hermans, "A model of the spatiotemporal characteristics of alpha rhythm," *Bull. Math. Biol.*, vol. 44, pp. 283–305, 1982.
[30] F. H. Lopes da Silva, "Dynamics of the electrical activity of the brain, local networks, and modulating systems," in *Neocortical Dynamics and Human EEG Rhythms, P. L. Nunez.* New York: Oxford Univ. Press, 1995,
[31] P. L. Nunez, "The brain wave equation: A model for the EEG," *Math. Biosci.*, vol. 21, pp. 279–297, 1974.
[32] R. D. Katznelson, "Normal modes of the brain: Neuranatomical basis and a physiological theoretical model," in *Electric Fields of the Brain: The Neurophysics of EEG*, P. L. Nunez. New York: Oxford Univ. Press, 1981,
[33] P. L. Nunez, "Generation of human EEG by a combination of short and long range neocortical interactions," *Brain Topogr.*, vol. 1, pp. 199–215, 1989.
[34] L. Ingber, "Statistical mechanics of multiple scales of neocortical interactions," in *Neocortical Dynamics and Human EEG Rhythms*, P. L. Nunez, Ed. New York: Oxford Univ. Press, 1995, pp. 628–681.
[35] G. Pfurtscheller and R. Cooper, "Frequency dependence of the transmission of EEG from cortex to scalp," *Electroencephalogr., Clin. Neurophysiol.*, vol. 42, pp. 817–826, 1975.

Ramesh Srinivasan received the B.S. degree in electrical engineering from the University of Pennsylvania, Philadelphia, in 1988 and the Ph.D. degree in biomedical engineering from Tulane University, New Orleans, LA, in 1995.

He spent two years as a National Institutes of Mental Health (NIMH)-sponsored Postdoctoral Fellow at the Institute of Cognitive and Decision Sciences at the Psychology Department of the University of Oregon, Eugene. He worked as a Scientist at Electrical Geodesics, Inc. (EGI), a manufacturer of commercial EEG systems in Eugene, OR. Currently, he is a Theoretical Fellow of the Neurosciences Institute in San Diego, CA and continues to consult with EGI. His current research interests are in the large-scale dynamics of human brain activity assessed with electroencephalography and steady-state evoked magnetic fields.

Paul L. Nunez received the Ph.D. degree in engineering science (engineering physics) and National Institutes of Health (NIH) sponsored postdoctoral training in the neurosciences, both from the University of California at San Diego.

He has worked in academic and industrial positions on spaceflight, controlled fusion (hot) and electroencephalography. He is currently a Professor of Biomedical Engineering and Director of the Brain Physics Group at Tulane University, New Orleans, LA. His current scientific interests encompass theoretical and experimental aspects of electroencephalography, including inverse problems, signal processing, nonlinear dynamics, cognitive studies, and medical applications. He is the author of two books: *Electric Fields of the Brain: The Neurophysics of EEG* (New York: Oxford Univ. Press, 1981) and *Neocortical Dynamics and Human EEG Rhythms*, (New York: Oxford Univ. Press, 1995).

Richard B. Silberstein received the B.S. degree (Honors) in physics from Monash University, Melbourne, in 1968 and the Ph.D. degree in neurophysiology from Melbourne University, Melbourne, Australia, in 1974.

He is currently Professor and Director of the Brain Sciences Institute at Swinburne University, Melbourne, Australia. His research interests include steady-state visually evoked potential probes of cognitive function and neocortical models of the electroencephalogram.